

The Web of Micro-Structures in IC 4593

M. Belén Mari ^{1,*}, Denise R. Gonçalves ¹ and Stavros Akras ² 

¹ Observatório do Valongo, Universidade Federal do Rio de Janeiro, Rio de Janeiro 20080-090, Brazil; denise@astro.ufrj.br

² Instituto de Matemática, Estatística e Física, Universidade Federal do Rio Grande, Rio Grande 96203-900, Brazil; stavrosakras@gmail.com

* Correspondence: mbmari@astro.ufrj.br

Received: 6 March 2020; Accepted: 25 May 2020; Published: 30 May 2020



Abstract: In addition to large-scale structures, planetary nebulae (PNe) show small-scale structures that emit mainly in low-ionization species such as [N II], [S II], [O II], and [O I], known as LISs. Here, we present the analysis of optical long-slit spectra, for three slit positions, of the PN IC 4593, which possesses a pair of knots and an isolated low-ionization knot. The motivation for this work is the need to characterize LISs completely to evaluate their impact on the PNe studies. These data allow us to derive the physical properties and ionization state for each morphological component of the nebula, including its pair of knots and individual knot. Due to the large uncertainties in the [S II] derived electron densities, we cannot confirm any contrast between the LISs' electron densities and the surrounding nebula, found in numerous other LISs. Though the lack of spatially-resolved physical parameters in the literature prevents further comparisons, in general, our results derived for the entire nebula agree with previous studies.

Keywords: ISM; planetary nebulae; individual; IC 4593

1. Introduction

Planetary nebulae (PNe) are the products of stellar wind interactions, at the latest stages on the evolution of low- and intermediate-mass stars. The schematic view of PNe can be given by their large-scale structures such as rims, shells, halos, and for a significant number of them, also by their small-scale, low-ionization ([N II], [S II], [O II], and [O I]) structures (LISs) (e.g., [1–5]).

LISs appear in a variety of morphologies: knots (isolated or in pairs), filaments, jets, and jet-like structures, of low ionization, attached to or detached from the main shells of the nebulae [3]. Previously, more acronyms were attributed to LISs by different authors: fast, low-ionization emission regions (FLIERS; [6]); bipolar, rotating, episodic jets (BRETs; [7]); or slowly moving low-ionization emitting regions (SLOWERS; [8]). Their physical properties, like electron temperature (T_e), electron density (N_e), and chemical composition (ionic and total abundances) have been extensively studied by several groups. Some overall conclusions are: (1) There is no significant difference in the T_e between LISs and the surrounding nebular medium. (2) LISs' N_e is found to be systematically lower than or equal to the electron densities of the surrounding nebular medium. (3) There is no overabundance of any element in LISs, as compared to the rest of the nebula. (4) The total mass of LISs must be mostly neutral, in order to overcome the discrepancy between the model predicted and the observed electron densities (e.g., [2,4–6,9–16]).

Though several studies have been carried out in order to explore the ionization structure of the different nebular components, with the aim to disentangle the excitation mechanism of LISs (stellar UV radiation and/or shocks), the results are not robust enough, and the issue deserves much more attention. In this work, we present the preliminary results from the spectroscopic analysis of IC 4593, a planetary nebula with a complex morphology that possesses a system of asymmetrical

shells and LISs (pairs and isolated knots). Here, we follow [17] for the morphological nomenclature (Figure 1).

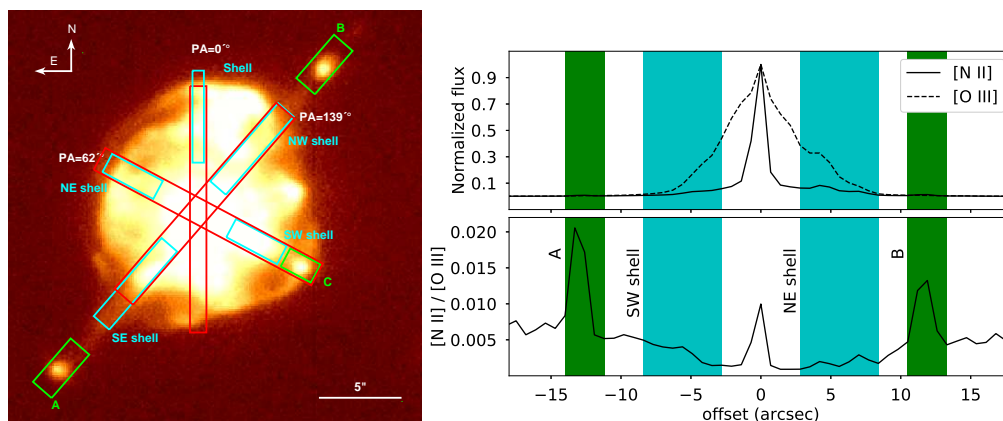


Figure 1. **Left:** The [N II] image of IC 4593, from [18], on which the extraction windows of the different components are superposed as boxes, for the integrated emission (Neb; in red), the shells (in cyan), and the low-ionization species (LISs) (A, B, and C; in green). The extension of these nebular components are as follows. Neb has the same extension in all directions, 15 arcsec. PA = 0°: 5.6 arcsec, shell. PA = 62°: 3.5 arcsec, shells; 2.1 arcsec, C. PA = 139°: 6.3 arcsec, shells; 3.5 arcsec, for A and B. The slit lengths are >13.7 arcmin for PA = 0° and 4 arcmin for PAs 62° and 139°. **Right:** The spatial profile of the [N II] and [O III] emission lines, normalized to 1.0, and the [N II]/[O III] line ratio, along the 139° slit.

2. Observations

Optical spectroscopic data of IC 4593 were obtained using the Intermediate Dispersion Spectrograph (IDS), on the 2.54 m Isaac Newton Telescope (INT), at the Observatorio del Roque de los Muchachos, in Spain, and the Danish Faint Object Spectrograph and Camera (DFOSC), on the 1.54 m Danish telescope, at the European Southern Observatory (ESO), La Silla, Chile. For the IDS, the R300V grating and the TEK5 CCD camera, as well as a slit of 1.5 arcsec width and 4 arcmin length were used, resulting in a dispersion of $3.3 \text{ \AA pixel}^{-1}$, in the spectral range between 3650 and 7000 \AA , and a spatial scale of $0.70 \text{ arcsec pixel}^{-1}$. The DFOSC was equipped with the 2000 \times 2000 CCD camera with a 15 μm pixel size. Grism #4 (300 lines mm^{-1}) was selected together with a 1.0 arcsec slit width and >13.7 arcmin length, covering from 3600 to 8000 \AA in wavelength, with a dispersion of $2.2 \text{ \AA pixel}^{-1}$, and a pixel size of 0.4 arcsec.

Three different position angles (P.A.) were selected: 0°, obtained with DFOSC, on 12 April 1997; 62° and 139°, observed with IDS, on 29 August 2001. In Figure 1, we show the [N II] image of IC 4593, superposed with the extraction windows of the nebular structures analyzed in this work.

3. Preliminary Results and Discussion

In order to explore the ionization structure of IC 4593, in a spatially-resolved fashion, individual spectra were extracted from the different PAs (see Figure 1). The emission-line fluxes, as well as the interstellar extinction, $c(\text{H}\beta)$, N_e , and T_e were determined and are presented in Table 1, for the position angles 0° and 62°, and in Table 2, for PA 139°. The nebular components analyzed here were: (i) the pair of knots, A and B (PA of 139°); (ii) the individual knot, C (PA of 62°); (iii) the shells (all PAs); and (iv) the Neb, the integrated emission, in all directions.

$c(\text{H}\beta)$, the interstellar extinction, was found to vary from 0.05 to 0.16 in the entire nebula. The average value was 0.10 ± 0.01 , which was in good agreement with the values reported in previous works (e.g., 0.08 ± 0.21 [19], 0.125 ± 0.041 [20] and 0.24 ± 0.16 [21]). In fact, by inspecting the tables, we see that this parameter varied from one to another structure and direction, which suggested real extinction variation within the object.

T_e [O III] had values between ~ 7500 and $10,000$ K, very much in agreement with [19–22], who obtained, respectively, 8700 , 9200 ± 500 , 8900 , and 8500^{+300}_{-200} K for the [O III] temperature of IC 4593. For T_e [N II], we derived values from ~ 8800 to $\sim 12,300$ K, again in good agreement with [21,22], which reported [N II] electron temperatures of $11,400$ and 9700^{+1300}_{-900} K, respectively. As in the Introduction, many authors reached the same conclusion that the electron temperatures of the PNe that contained LISs were roughly homogeneous for all nebular components, a trend that was also clearly present in our study of IC 4593.

Regarding the electron densities, N_e [S II] was found to assume values between ~ 2000 and $\sim 2300 \text{ cm}^{-3}$, while [19–21] found the following: 1860 , 2000 ± 1500 and $2000^{+700}_{-500} \text{ cm}^{-3}$, respectively. Unfortunately, N_e was based solely on the [S II] doublet, which was very faint in all structures of this nebula, leading to these poor results with error bars on N_e too large to draw any conclusions about the difference in electron density between the LISs and the nebula.

On the other hand, as anticipated in the Introduction, several authors have reported similar trends, implying that LISs have lower or at least equal electron densities, if compared to those derived for the surrounding medium (e.g., [5,6,9,11]).

LISs' electron density comparisons are particularly interesting because they pinpoint the need to understand if there is a real contradiction between theoretical models and observations. Perhaps, by turning attention to the molecular gas and dust components, this controversy between results and models disappears. Actually, recent observations have unveiled that LISs in PNe are also made of molecular hydrogen (H_2) (e.g., [15,16,23–25]). These discoveries have provided a confirmation of the scenario proposed by [11] that LISs are dense molecular structures similar to the cometary knots of PNe like Helix and Dumbbell [26,27]; see Akras et al.'s contribution in [28]).

Table 1. Results for position angles 0° and 62° . Percentage errors are given within parentheses.

	PA = 0°		PA = 62°			
	Neb 15''	Shell 5.6''	Neb 15''	NE Shell 3.5''	SW Shell 3.5''	C 2.1''
$\log F$ ($\text{H}\beta$)	−11.44	−12.09	−11.22	−12.30	−11.64	−13.04
c ($\text{H}\beta$)	0.16 ± 0.02	0.05 ± 0.01	0.05 ± 0.01	0.00 ± 0.01	0.00 ± 0.01	0.01 ± 0.02
N_e [S II] (cm^{-3})	2010 (>50%)	1870 (30%)	5920 (>50%)	1700 (45%)	2130 (31%)	1900 (47%)
T_e [O III] (K)	7980 (4%)	7530 (3%)	7870 (5%)	8240 (4%)	8180 (2%)	8670 (8%)
T_e [N II] (K)	-	9570 (16%)	8760 (24%)	10,000 (19%)	8950 (8%)	9590 (21%)

Table 2. Results for position angle 139° . Percentage errors are given within parentheses.

	PA = 139°				
	Neb 15''	A 3.5''	SE Shell 6.3''	NW Shell 6.3''	B 3.5''
$\log F$ ($\text{H}\beta$)	−11.21	−13.64	−12.07	−11.43	−13.53
c ($\text{H}\beta$)	0.08 ± 0.02	0.24 ± 0.07	0.24 ± 0.01	0.07 ± 0.02	0.12 ± 0.10
N_e [S II] (cm^{-3})	2310 (>50%)	2000 (>50%)	1810 (46%)	1460 (>50%)	1800 (49%)
T_e [O III] (K)	8660 (5%)	8920 (28%)	8030 (3%)	8980 (5%)	9990 (18%)
T_e [N II] (K)	10,520 (27%)	12,260 (28%)	9770 (20%)	9440 (25%)	9550 (21%)

4. Future Work

It is clear that more PNe need to be spectroscopically observed with high SNR in order to explore the electron density differences of LISs in contrast with other nebular components. Hen 2-429, NGC 6543, NGC 6905, Hen 2-186, and NGC 3918 are presently under analysis in our sample. In most of the cases, spectra are deep enough to allow more robust results about the electron density contrasts, as well, and will be published in forthcoming papers.

In connection with the need to investigate the non-ionized content of LISs, the work in [29] concluded that the missing mass problem in PNe could be unscrambled with more accurate data of molecular gas, since otherwise, we would be restricted to only the ionized mass. In fact, the cometary knots in the Helix nebula can be good examples of this absence of information applied to the case of LISs (see [30]). Moreover, one of the Helix cometary knots was demonstrated to have a molecular-to-ionized mass ratio of $\sim 10^5$ [31,32], or even a higher ratio according to the more recent CO observations [33]. To further illustrate how much additional mass can be hidden in the form of dust and molecules (H_2 + CO) in the cometary knots of the Helix nebula, see [34] and [32,33], respectively.

Therefore, besides the study of the aforementioned nebulae and their LISs in the optical regime, it is also necessary to obtain new data in the near-IR and millimeter wavelengths and study their molecular content (H_2 and CO). So far, excluding a couple of PNe with cometary knots, H_2 was detected in another six PNe with LISs (see [15,16] and the references therein). It is still an open question whether, besides the Helix cometary knot, the other LISs are also made of cold CO gas. Such observations would allow us to tackle the LISs' missing mass problem by measuring the amount of molecular mass in the two most abundant molecules, H_2 and CO.

5. Conclusions

In this contribution we discussed the physical properties ($c(H\beta)$, N_e and T_e) of IC 4593, obtained from the optical spectra of its shells and LISs (a pair of knots and an isolated knot) as well as of the entire nebula, for three different position angles.

Regarding the extinction coefficient, the minimal and maximum values are 0.05 to 0.16 and we found the average of 0.10 ± 0.01 , which, as in the case of T_e and N_e for the entire nebula, are in good agreement with previous works. Moreover, our results show that this nebula has significant variation of the extinction from one to another component and direction. Regarding the electron temperatures, we have shown that T_e are homogeneous along all directions of the nebulae, no matter if considering its shells or low-ionization knots, and amount to 8000 – 9000K for $T_e[O\text{ III}]$, and 9000 – 10000K for $T_e[N\text{ II}]$. Due to the large $N_e[S\text{ II}]$ uncertainties, when comparing one to another component of IC 4593, we cannot give as robust conclusions as for T_e . Although face values of 2000 cm^{-3} [S II] electron densities were found indistinctly for the LISs and the surrounding medium, following a trend found in previous spatially resolved studies of PNe that contain low-ionization knots.

Despite the results presented here, clearly much more such kinds of analysis are needed for PNe with all the diversity of LISs' types and for different wavelength ranges (near-IR and millimeter). Only then we will achieve a complete understanding of the physical processes that result in the formation of the various types of LIS.

Author Contributions: M.B.M., writing-original draft and revision's editing; D.R.G. and S.A., validation and critical review. All authors have read and agreed to the published version of the manuscript.

Funding: This research was funded by CAPES and CNPq.

Acknowledgments: M.B.M. acknowledges the support of CAPES—the Federal Agency for Support and Evaluation of Graduate Education within the Ministry of Education of Brazil. D.R.G. acknowledges the partial support by CNPq Grants 304184/2016-0 and 428330/2018-5.

Conflicts of Interest: The authors declare no conflict of interest. The funders had no role in the design of the study; in the collection, analyses, or interpretation of data; in the writing of the manuscript; nor in the decision to publish the results.

References

1. Corradi, R.L.M.; Manso, R.; Mampaso, A.; Schwarz, H.E. Unveiling low-ionization microstructures in planetary nebulae. *Astron. Astrophys.* **1996**, *313*, 913–923.
2. Balick, B.; Alexander, J.; Hajian, A.R.; Terzian, Y.; Perinotto, M.; Patriarchi, P. FLIERs and Other Microstructures in Planetary Nebulae. IV. Images of Elliptical PNs from the Hubble Space Telescope. *Astron. J.* **1998**, *116*, 360–371. [[CrossRef](#)]

3. Gonçalves, D.R.; Corradi, R.L.M.; Mampaso, A. Low-Ionization Structures in Planetary Nebulae: Confronting Models with Observations. *Astrophys. J.* **2001**, *547*, 302–310. [[CrossRef](#)]
4. Gonçalves, D.R.; Corradi, R.L.M.; Mampaso, A.; Perinotto, M. The Physical Parameters, Excitation, and Chemistry of the Rim, Jets, and Knots of the Planetary Nebula NGC 7009. *Astrophys. J.* **2003**, *597*, 975–985. [[CrossRef](#)]
5. Akras, S.; Gonçalves, D.R. Low-ionization structures in planetary nebulae—I. Physical, kinematic and excitation properties. *Mon. Not. R. Astron. Soc.* **2016**, *455*, 930–961. [[CrossRef](#)]
6. Balick, B.; Rugers, M.; Terzian, Y.; Chengalur, J.N. Fast, Low-Ionization Emission Regions and Other Microstructures in Planetary Nebulae. *Astrophys. J.* **1993**, *411*, 778. [[CrossRef](#)]
7. Lopez, J.A.; Vazquez, R.; Rodriguez, L.F. The Discovery of a Bipolar, Rotating, Episodic Jet (BRET) in the Planetary Nebula KJpN 8. *Astrophys. J.* **1995**, *455*, L63. [[CrossRef](#)]
8. Perinotto, M. Gas Dynamics in Planetary Nebulae: From Macro-structures to FLIERs. *Astrophys. Space Sci.* **2000**, *274*, 205–219. [1026516527132](#). [[CrossRef](#)]
9. Hajian, A.R.; Balick, B.; Terzian, Y.; Perinotto, M. FLIERs and Other Microstructures in Planetary Nebulae. III. *Astrophys. J.* **1997**, *487*, 304–313. [[CrossRef](#)]
10. Gonçalves, D.R.; Mampaso, A.; Corradi, R.L.M.; Perinotto, M.; Riera, A.; López-Martín, L. K 4-47: A planetary nebula excited by photons and shocks. *Mon. Not. R. Astron. Soc.* **2004**, *355*, 37–43. [[CrossRef](#)]
11. Gonçalves, D.R.; Mampaso, A.; Corradi, R.L.M.; Quireza, C. Low-ionization pairs of knots in planetary nebulae: Physical properties and excitation. *Mon. Not. R. Astron. Soc.* **2009**, *398*, 2166–2176. [[CrossRef](#)]
12. Leal-Ferreira, M.L.; Gonçalves, D.R.; Monteiro, H.; Richards, J.W. Physico-chemical spectroscopic mapping of the planetary nebula NGC 40 and the 2D_NEb, a new 2D algorithm to study ionized nebulae. *Mon. Not. R. Astron. Soc.* **2011**, *411*, 1395–1408. [[CrossRef](#)]
13. Monteiro, H.; Gonçalves, D.R.; Leal-Ferreira, M.L.; Corradi, R.L.M. Spatially resolved physical and chemical properties of the planetary nebula NGC 3242. *Astron. Astrophys.* **2013**, *560*, A102. [[CrossRef](#)]
14. O’Dell, C.R.; Balick, B.; Hajian, A.R.; Henney, W.J.; Burkert, A. Knots in Nearby Planetary Nebulae. *Astron. J.* **2002**, *123*, 3329–3347. [[CrossRef](#)]
15. Akras, S.; Gonçalves, D.R.; Ramos-Larios, G. H₂ in low-ionization structures of planetary nebulae. *Mon. Not. R. Astron. Soc.* **2017**, *465*, 1289–1296. [[CrossRef](#)]
16. Akras, S.; Gonçalves, D.R.; Ramos-Larios, G.; Aleman, I. H₂ Emission in the Low-Ionisation Structures of the Planetary Nebulae NGC 7009 and NGC 6543. *Mon. Not. R. Astron. Soc.* **2020**, *493*, 3800–3810. [[CrossRef](#)]
17. Corradi, R.L.M.; Guerrero, M.; Machado, A.; Mampaso, A. Multiple collimated outflows in a planetary nebula? *New Astron.* **1997**, *2*, 461–470. [[CrossRef](#)]
18. Machado, A.; Guerrero, M.A.; Stanghellini, L.; Serra-Ricart, M. The IAC Morphological Catalog of Northern Galactic Planetary Nebulae. In Proceedings of the 180th Symposium of the IAU, Groningen, The Netherlands, 26–30 August 1996.
19. Cahn, J.H. Interstellar extinction: A calibration by planetary nebulae. *Astron. J.* **1976**, *81*, 407–418. [[CrossRef](#)]
20. Barker, T. Spectrophotometry of planetary nebulae. I. Physical conditions. *Astrophys. J.* **1978**, *219*, 914–930. [[CrossRef](#)]
21. Delgado Inglada, G.; Rodríguez, M.; Mampaso, A.; Viironen, K. The Iron Abundance in Galactic Planetary Nebulae. *Astrophys. J.* **2009**, *694*, 1335–1348. [[CrossRef](#)]
22. Kaler, J.B. Electron Temperatures in Planetary Nebulae. *Astrophys. J.* **1986**, *308*, 322. [[CrossRef](#)]
23. Fang, X.; Guerrero, M.A.; Miranda, L.F.; Riera, A.; Velázquez, P.F.; Raga, A.C. Hu 1-2: A metal-poor bipolar planetary nebula with fast collimated outflows. *Mon. Not. R. Astron. Soc.* **2015**, *452*, 2445–2462. [[CrossRef](#)]
24. Fang, X.; Zhang, Y.; Kwok, S.; Hsia, C.H.; Chau, W.; Ramos-Larios, G.; Guerrero, M.A. Extended Structures of Planetary Nebulae Detected in H₂ Emission. *Astrophys. J.* **2018**, *859*, 92. [[CrossRef](#)]
25. Machado, A.; Stanghellini, L.; Villaver, E.; García-Segura, G.; Shaw, R.A.; García-Hernández, D.A. High-resolution Imaging of NGC 2346 with GSAOI/GeMS: Disentangling the Planetary Nebula Molecular Structure to Understand Its Origin and Evolution. *Astrophys. J.* **2015**, *808*, 115. [[CrossRef](#)]
26. Matsuura, M.; Speck, A.K.; McHunu, B.M.; Tanaka, I.; Wright, N.J.; Smith, M.D.; Zijlstra, A.A.; Viti, S.; Wesson, R. A “Firework” of H₂ Knots in the Planetary Nebula NGC 7293 (The Helix Nebula). *Astrophys. J.* **2009**, *700*, 2. [[CrossRef](#)]
27. Baldrige, S.P. Small—scale Structures in Planetary Nebulae. Ph.D. Thesis, University of Missouri, Columbia, MO, USA, 2017.

28. Akras, S.; Gonçalves, D.R.; Ramos-Larios, G.; Aleman, I. Molecular Hydrogen Microstructures in Planetary Nebulae. *Galaxies* **2020**, *8*, 30. [[CrossRef](#)]
29. Kimura, R.K.; Gruenwald, R.; Aleman, I. Molecular chemistry and the missing mass problem in planetary nebulae. *Astron. Astrophys.* **2012**, *541*, A112. [[CrossRef](#)]
30. Matsuura, M.; Speck, A.K.; Smith, M.D.; Zijlstra, A.A.; Viti, S.; Lowe, K.T.E.; Redman, M.; Wareing, C.J.; Lagadec, E. VLT/near-infrared integral field spectrometer observations of molecular hydrogen lines in the knots of the planetary nebula NGC 7293 (the Helix Nebula). *Mon. Not. R. Astron. Soc.* **2007**, *382*, 1447–1459. [[CrossRef](#)]
31. O'dell, C.R.; Handron, K.D. Cometary Knots in the Helix Nebula. *Astron. J.* **1996**, *111*, 1630. [[CrossRef](#)]
32. Huggins, P.J.; Forveille, T.; Bachiller, R.; Cox, P.; Ageorges, N.; Walsh, J.R. High-Resolution CO and H₂ Molecular Line Imaging of a Cometary Globule in the Helix Nebula. *Astrophys. J. Lett.* **2002**, *573*, L55–L58. [[CrossRef](#)]
33. Andriantsaralaza, M.; Zijlstra, A.; Avison, A. CO in the C1 globule of the Helix nebula with ALMA. *Mon. Not. R. Astron. Soc.* **2020**, *491*, 758–772. [[CrossRef](#)]
34. Meaburn, J.; Walsh, J.R.; Clegg, R.E.S.; Walton, N.A.; Taylor, D.; Berry, D.S. Dust in the neutral globules of the Helix nebula, NGC 7293. *Mon. Not. R. Astron. Soc.* **1992**, *255*, 177–182. [[CrossRef](#)]



© 2020 by the authors. Licensee MDPI, Basel, Switzerland. This article is an open access article distributed under the terms and conditions of the Creative Commons Attribution (CC BY) license (<http://creativecommons.org/licenses/by/4.0/>).